ADVANCED OPTICAL MATERIALS
www.advopticalmat.de

High-Efficiency Mutual Dual-Band Asymmetric Transmission of Circularly Polarized Waves with Few-Layer Anisotropic Metasurfaces

Jieying Liu, Zhancheng Li, Wenwei Liu, Hua Cheng, Shuqi Chen, and Jianguo Tian**

Metasurfaces are periodic 2D artificial media with subwavelength unit cells and thicknesses, which overcome physical limitations imposed by natural materials and are able to guide electromagnetic waves in unprecedented ways with great precision.[1–4] Numerous applications based on metasurfaces have been proposed such as ultrathin lenses,[5,6] high-resolution holograms,[7] vector beam generators,[8,9] refractive quarter-wave plates,[10] and anomalous refraction.[11] Recently, a Lorentz reciprocal phenomenon in metasurfaces termed asymmetric transmission, first investigated by Fedotov et al., has attracted much interest.[12] The effect manifests itself as a difference in the total transmission between forward and backward propagation and can be realized with the aid of polarization conversion.

Asymmetric transmission effects with metasurfaces for both linearly polarized waves and circularly polarized waves have been proposed.[13–24] These designs can be used as polarization transformers and polarization-controlled devices for applications in spectroscopy, ultrafast information processing, optical interconnects, communications, and so on. In particular, asymmetric transmission of circularly polarized waves has attracted much attention and has been realized in single-layer metasurfaces. For example, Fedotov et al. achieved asymmetric transmission of circularly polarized waves at normal incidence with a planar split-ring microwave metamaterial.[20] However, the limited interaction between waves and single-layer metasurfaces reduced the efficiency and bandwidth of the asymmetric transmission, preventing their practical applications.

Recent advances in few-layer metasurfaces provide an alternative way to overcome the drawbacks of single-layer metasurfaces. Wu et al. proposed two different bilayered chiral metamaterials to enhance the asymmetric transmission effects of circularly polarized GHz waves.[23] Pfeiffer et al. experimentally demonstrated that three-layer bianisotropic metasurfaces allow for high-performance polarization control of light.[24] Few-layer metasurfaces with near-field wave interference and resonances between layers improve the asymmetric transmission efficiency of circular polarization and provide the intriguing possibility of its real application. Although previous approaches in few-layer metasurfaces dramatically enhanced the efficiency of single-band asymmetric transmission of circular polarization, manipulation of this effect and expansion of the working bandwidth is still inherently difficult. The few-layer metasurfaces in previous works have the complicated structure parameters and the high requirement of structure alignments, which prevent them from real applications. Moreover, multiband operation of high-efficiency asymmetric transmission of circularly polarized waves is still highly desirable for novel applications such as multiband polarizers and filters.

The anisotropic of the metasurface structure is vital for generating asymmetric transmission. Thus, metasurfaces with both anisotropic and few-layer structures are expected to perform well in asymmetric transmission applications. Here, we propose a three-layer anisotropic metasurface by stacking multilayers of rotated gold nanorods that can realize high-efficiency dual-band asymmetric transmission and mutual polarization conversion for circularly polarized waves in the near-infrared regime. Moreover, it can, respectively, transform left-circularly polarized (LCP) and right-circularly polarized (RCP) incident waves to orthogonally polarized waves in two adjacent wavebands within a single propagation direction. The superior cross-polarization conversion is attributed to Fabry–Pérot-like resonance cavities formed between three metallic layers and the air–Si_3N_4 interface. The high-performance asymmetric transmission results from the anisotropy of the structure and multiple reflection and transmission interference in the Fabry–Pérot-like resonance cavities, which was verified by performing wave-transfer matrix method. We find that the metasurface reaches opposite asymmetric transmission peaks of about 60% efficiency at 122.5 and 183.1 THz. In addition, orthogonal polarization conversion can be realized in two bands with more than 90% polarization conversion ratio (PCR) and conversion intensities of 0.54 and 0.40 are realized for normally incident LCP and RCP waves at around 172.5 and 133.8 THz, respectively.

An artistic rendering of the asymmetric transmission in the proposed metasurface is presented in **Figure 1**a. A forward-incident LCP wave can be transmitted and transformed into an RCP wave, while a backward-incident LCP wave is mainly reflected in the higher frequency band. Figure 1b shows a unit cell of the three-layer anisotropic metasurface, which consists of three gold nanorods embedded in the Si_3N_4 substrate. The top (green) and bottom (red) nanorods are parallel to the x-axis, and the angle ϕ between the middle and top nanorods is 45°. The nanorods have dimensions of length L = 600 nm, width W = 250 nm, and thickness t = 40 nm, with a layer-to-layer

Dr. J. Liu, Dr. Z. Li, Dr. W. Liu, Prof. H. Cheng, Prof. S. Chen, Prof. J. Tian
The Key Laboratory of Weak Light Nonlinear Photonics
Ministry of Education
School of Physics and TEDA Institute of Applied Physics
Nankai University
Tianjin 300071, China
E-mail: schen@nankai.edu.cn; jjtian@nankai.edu.cn

DOI: 10.1002/adom.201600602

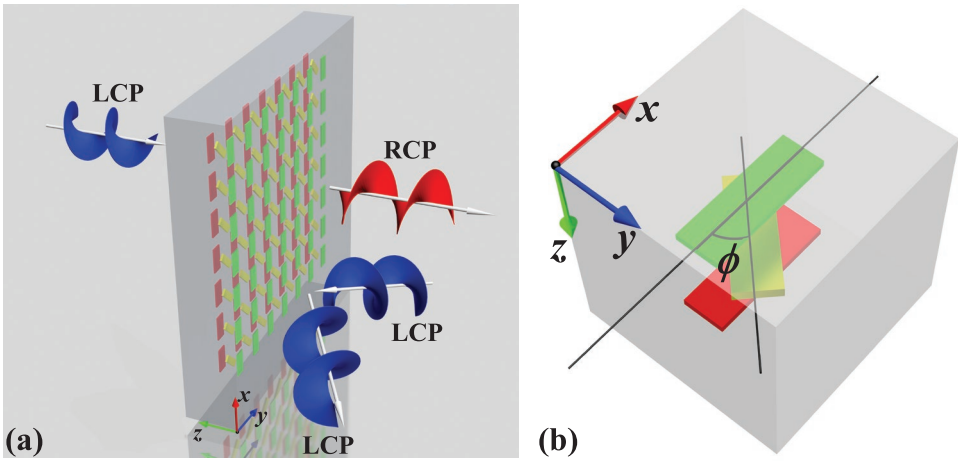

Figure 1. a) Artistic rendering of the asymmetric transmission for the proposed three-layer anisotropic metasurface. The circularly polarized waves can be transmitted and are converted into orthogonal polarization in one direction while they can be efficiently reflected in the other direction. b) Geometry detail of designed metasurface. The angle ϕ indicates the angle between the top (green) and the middle (yellow) nanorods.

separation distance d = 200 nm, and a period of the unit cell of P = 750 nm in both the x and y directions. The thickness of Si_3N_4 covered on the top nanorods is also d = 200 nm.

Numerical simulations have been conducted to analyze the characterizations of the proposed metasurface, using CST microwave studio.[25] In our simulations, unit-cell boundary conditions were used in the x and y directions, and an open (perfectly matched layer) boundary was defined in the z direction, while the excitation sources were LCP and RCP normally incident waves. The permittivity of the Si_3N_4 substrate was 4. The real part of the permittivity for Si_3N_4 almost keeps a constant in the near-infrared wavelength and depends fairly monotonically on the flow rate of N_2 in the fabrication process. When the frequency is lower than 300 THz, the imaginary part of the permittivity is almost equal to zero. Therefore, the permittivity of Si_3N_4 is set to be a constant in our simulation. The dispersion function of gold was defined by the Drude model with plasma frequency $\omega_p = 1.37\times10^{16}\,s^{-1}$ and damping constant $\gamma = 4.08\times10^{13}\,s^{-1}$.[26] To account for surface scattering, grain boundary effects in the thin gold film, and inhomogeneous broadening, we used a three times higher damping constant than bulk.[18,24,27,28] Different damping constants will affect the peak value of asymmetric transmission. With the increasing of the damping constant, the peak value of asymmetric transmission will be gradually decreasing.

The Jones matrix[29,30] is introduced to analyze the asymmetric transmission of circularly polarized waves. For the circular base, the generally complex amplitudes of the incident field and the transmitted field can be related by complex Jones matrices **T**:

$$\begin{pmatrix} T_{LCP} \\ T_{RCP} \end{pmatrix} = \begin{pmatrix} T_{LL} & T_{LR} \\ T_{RL} & T_{RR} \end{pmatrix} \begin{pmatrix} I_{LCP} \\ I_{RCP} \end{pmatrix} = \mathbf{T}^{f}_{circ} \begin{pmatrix} I_{LCP} \\ I_{RCP} \end{pmatrix} \quad (1)$$

The superscript "f" indicates forward propagation (along the +z direction). Since the structure does not contain any magnetooptic material, the reciprocity theorem is applied and the Jones matrix **T** for backward propagation can be written as

$$\mathbf{T}^{b}_{circ} = \begin{pmatrix} T_{LL} & T_{RL} \\ T_{LR} & T_{RR} \end{pmatrix} \quad (2)$$

Thus, the total transmission of an LCP wave is

$$t^{f} = |T_{LL}|^2 + |T_{RL}|^2 \quad (3a)$$

$$t^{b} = |T_{LL}|^2 + |T_{LR}|^2 \quad (3b)$$

The asymmetric transmission is defined as the difference between the transmission of forward propagation and that of backward propagation, and can be expressed as

$$\Delta t = \Delta^{LCP}_{circ} = |T_{RL}|^2 - |T_{LR}|^2 = -\Delta^{RCP}_{circ} \quad (4)$$

We can see that the asymmetric transmission originates from the difference between the magnitudes of two cross-polarization transmission coefficients.

To obtain the transmission properties for the proposed metasurface, the squared moduli of four **T** matrix elements $t_{ij} = |T_{ij}|^2$ for forward (+z) and backward (−z) propagating waves are simulated and shown in **Figure 2**. Apparently, the two cross-polarization transmission coefficients exchange with each other when the propagation direction is reversed, while the copolarization transmission coefficients remain unchanged. According to Figure 2(a), t_{LR} and t_{RL} are extremely different for the two wavebands near 120 and 180 THz. The simulated asymmetric transmissions of LCP and RCP waves are presented in **Figure 3**a. The high-performance asymmetric transmission reaches two maximum values $\Delta^{LCP}_{circ} = 0.638$ and $\Delta^{RCP}_{circ} = 0.588$ at 183.1 and 122.5 THz, respectively. Thus, when circularly polarized waves in the lower waveband are incident along the forward direction, the RCP waves can pass through the metasurface while the LCP waves are forbidden. However, the case will be reversed when the incident waves are in the higher waveband or the propagation direction is reversed. The asymmetric transmission in the designed metasurface is attributed to the structural anisotropy with a mirror symmetry perpendicular to the z-axis and

Adv. Optical Mater. 2016,
DOI: 10.1002/adom.201600602

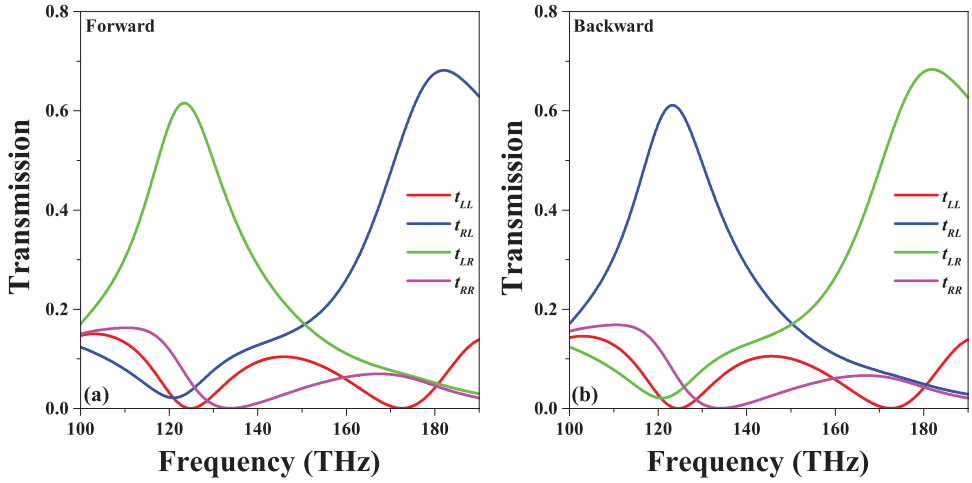

Figure 2. Simulated squared moduli $t_{ij} = |T_{ij}|^2$ of the **T** matrix for a) forward and b) backward incidence.

at most a C_2 symmetry with respect to the z axis.[29] In order to study the influence of anisotropy on the asymmetric transmission effect, we simulated asymmetric transmission of LCP waves in the metasurface with different values of ϕ, as shown in Figure 3b. By changing the angle ϕ to 0°, 15°, 30°, and 45°, the anisotropy is varied accordingly. The asymmetric transmission efficiency increases with increasing structural anisotropy, and when $\phi = 0°$, the structure becomes mirror symmetry with respect to the x–z and y–z plane and the asymmetric transmission vanishes.

The anisotropy of the structure also results in polarization conversion. As is shown in Figure 2a, the copolarization transmission coefficients are less than 0.2 spanning the entire considered frequency range and even decrease to nearly 0 at around 172.5 THz (LCP) and 133.8 THz (RCP). This suggests two polarization conversion wavebands realizing opposite polarization conversion. To measure the polarization conversion properties of the metasurface, we calculated the polarization conversion ratio (PCR) and ellipticity angle χ of transmitted field using

$$\mathrm{PCR}_j = \frac{t_{ij}}{t_{jj} + t_{ij}} \tag{5a}$$

$$\sin 2\chi = \frac{2r}{1+r^2}\sin\Delta\phi \tag{5b}$$

The results are plotted in **Figure 4**. The subscripts "j" and "i" denote the polarization states of the incident and transmitted waves, respectively. $\Delta\phi = \phi_y - \phi_x$ is the phase difference between the x- and y-components of the transmitted field, and $r = |E_y|/|E_x|$ is the ratio of the magnitudes of the x- and y-components of the transmitted field. As is known, PCR = 1 indicates complete polarization conversion, and χ = 45° and χ = −45° indicate that the transmitted field is RCP and LCP waves, respectively. For forward-incident LCP waves, the PCR is higher than 90% from 163.8 to 183 THz and the ellipticity angle is higher than 40° between 170.4 and 174.9 THz. At around 172.5 THz, complete polarization conversion from LCP to RCP is realized and the cross-polarization intensity is 0.54. The

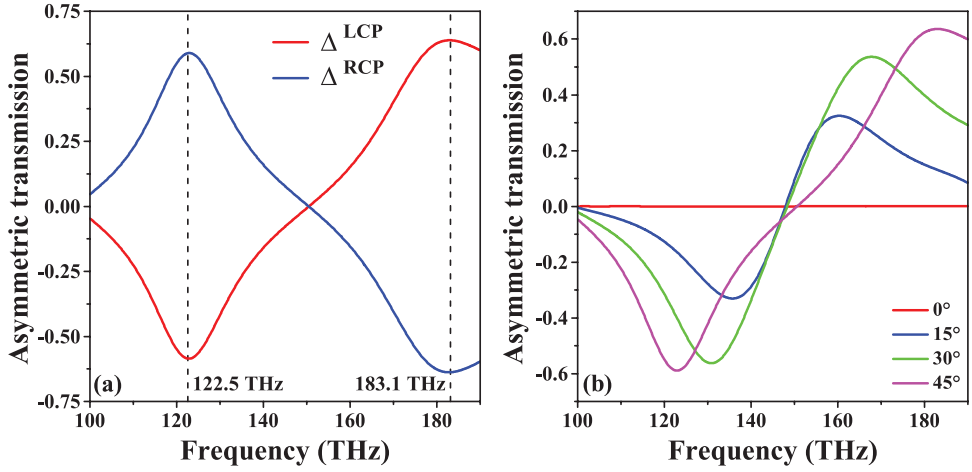

Figure 3. a) Simulated asymmetric transmission efficiency for LCP and RCP. b) Simulated asymmetric transmission efficiency for different values of the angle ϕ.

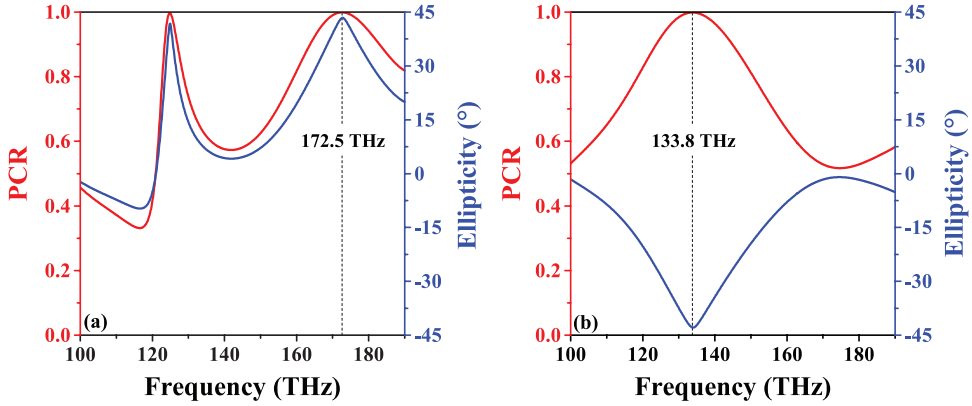

Figure 4. PCR and ellipticity angle χ of the transmission wave for a) LCP and b) RCP forward incidence.

maximum at 125 THz is not of significance because of the weak cross-polarization intensity of 0.03. As for RCP incidence, it is observed that complete polarization conversion from RCP to LCP is realized at 133.8 THz with a cross-polarization intensity of 0.40. Thus, the proposed metasurface has two polarization conversion wavebands corresponding to LCP-to-RCP and RCP-to-LCP, which is reversed in the case of backward incidence.

The enhanced asymmetric transmission in the dual-band and mutual polarization conversion can be attributed to the multiple reflection and transmission interference between the three metallic nanorod layers and the air–Si_3N_4 substrate interface, as shown in **Figure 5**a. To verify this interpretation, we simulated the transmission-matrix elements and reflection-matrix elements of every layer and performed wave-transfer

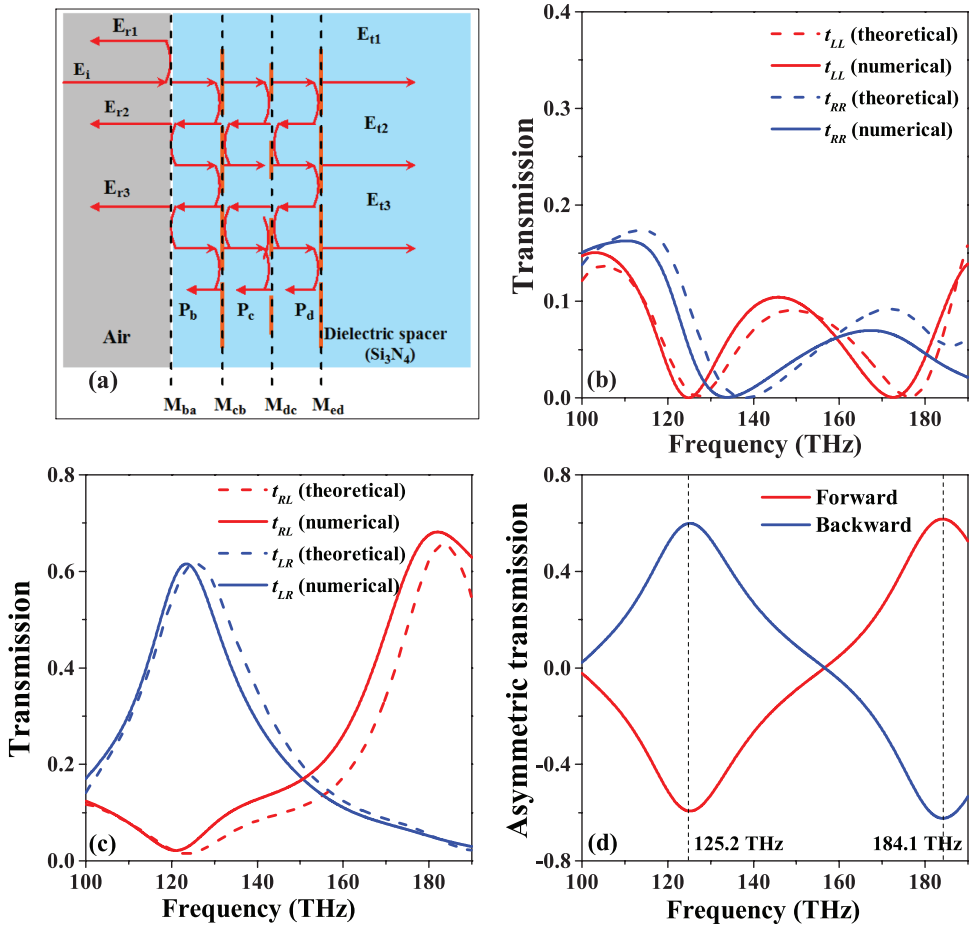

Figure 5. a) Schematic of the multiple reflection and transmission interference model in the three-layer metasurface. Simulated and calculated b) copolarization transmission coefficients and c) cross-polarization transmission coefficients of **T** matrix. d) Calculated asymmetric transmission for forward and backward incidence.

Adv. Optical Mater. **2016**,
DOI: 10.1002/adom.201600602

matrix method (denoted as 4 × 4 $\mathbf{M}_{ij}$ matrices) based on these data.[30,31] First, we simulated the scattering parameters (denoted as **T**-matrices and **R**-matrices) for every layer. Then, we calculated the scattering transfer parameters (denoted as **M**-matrices) based on the scattering parameters. The **M**-matrix $\mathbf{P}_i$ for a homogeneous medium with thickness d_i and refractive index n_i is given by

$$\mathbf{P}_i = \mathrm{diag}(e^{ik_0n_id_i}, e^{ik_0n_id_i}, e^{-ik_0n_id_i}, e^{-ik_0n_id_i}) \quad (6)$$

where k_0 is the wave number in free-space. Therefore, for the proposed structure, the overall **M**-matrix can be written as

$$\mathbf{M} = \mathbf{M}_{ed}\mathbf{P}_d\mathbf{M}_{dc}\mathbf{P}_c\mathbf{M}_{cb}\mathbf{P}_b\mathbf{M}_{ba} \quad (7)$$

Finally, the four elements of the transmission matrix were retrieved from the overall **M**-matrix.

The comparison of theoretically calculated and numerically simulated overall squared moduli of the four **T**-matrix elements for forward propagation are presented in Figure 5b,c, and the asymmetric transmission as determined by the theoretically calculated results is shown in Figure 5d. The calculated results agree well with those from the simulation. Owing to the nonignorable nanorod thickness, a tiny error was introduced in the multiple reflection and transmission interference model in which the metallic layer thickness is neglected, resulting in a slight blue-shift of about 2 THz in Figure 5b–d. The consistency of the simulation and calculation verify that the proposed model of multiple reflection and transmission interference is correct, and is suitable for the analysis and interpretation of the propagation properties of few-layer metasurfaces.

The multiple reflection and transmission interference in the metasurface releases the alignment requirement between adjacent layers of nanorods. The asymmetric transmission efficiencies for LCP waves of metasurfaces with misaligned nanorods are presented in **Figure 6**. The shift along the *x*- and *y*-axis between a misaligned layer and an accurately aligned layer is denoted as Δx and Δy, respectively. Figure 6a,b corresponds, respectively, to the shift of the top layer and middle layer. We considered four cases of misalignments: Δx = 0 nm, Δy = 0 nm (solid line); Δx = 15 nm, Δy = 0 nm (dashed line); Δx = 0 nm, Δy = 15 nm (short dashed line); and Δx = 15 nm, Δy = 15 nm (dotted line). The results show that limited shifts of the nanorods have almost no effect on the generation of asymmetric transmission, which is beneficial for its practical applications.

Our designs also release the high-precision requirements of the structure parameters, which benefit from the multiple interference in the few-layer metasurfaces. To display the influence of structure parameters on the proposed asymmetric transmission, we calculated the asymmetric transmissions with different structure parameters and separation distances in **Figure 7**. The length of the nanorod and the period of the metasurface have almost no effect on the asymmetric transmission (see Figure 7a,b). The width of the nanorod slightly affects the asymmetric transmission compared with the length and period (see Figure 7c). Basically, the variations of structure parameters in an appropriate range do not affect the asymmetric transmission. The variation of the separation distance has an apparent shift for the asymmetric transmission (see Figure 7d), since it is directly associated with the multiple interference in the few-layer metasurfaces.

In conclusion, we proposed high-efficiency dual-band asymmetric transmission with mutual polarization conversion for circularly polarized waves in the near-infrared regime with a few-layer anisotropic metasurface composed of three layers of gold nanorods embedded in the Si_3N_4 substrate. The results show that at around 120 and 180 THz, two opposite asymmetric transmission effects are realized with an asymmetric transmission efficiency of about 60%, which is attributed to the structural anisotropy of the metasurface. Moreover, the anisotropy also results in polarization conversion. Complete polarization conversion for LCP and RCP waves propagating along the forward direction is realized at 172.5 and 133.8 THz with cross-polarization transmission coefficients of 0.54 and 0.40, respectively. A model of multiple reflection and transmission interference was used to demonstrate the generation of high efficiency dual-band asymmetric transmission effects. This model was verified by a wave-transfer matrix method, and was shown to provide a

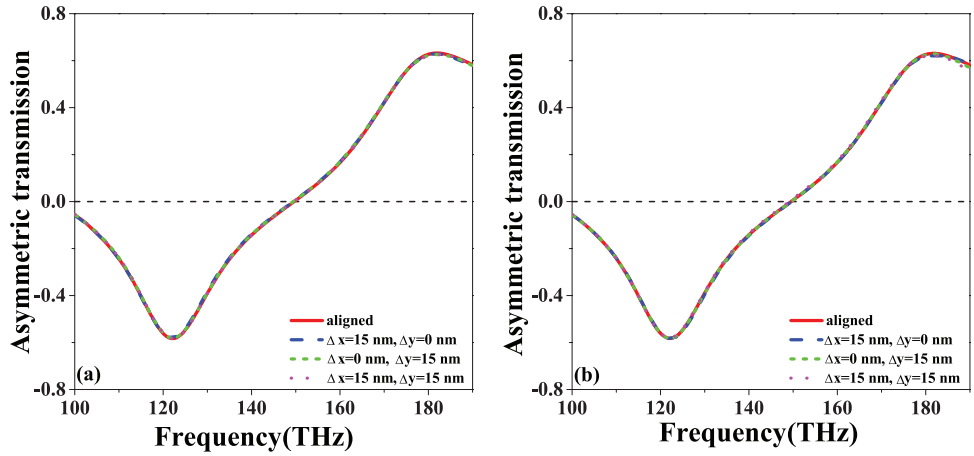

Figure 6. a) Asymmetric transmission for forward incidence with different location of top nanorods. b) Asymmetric transmission for forward incidence with different location of middle nanorods.

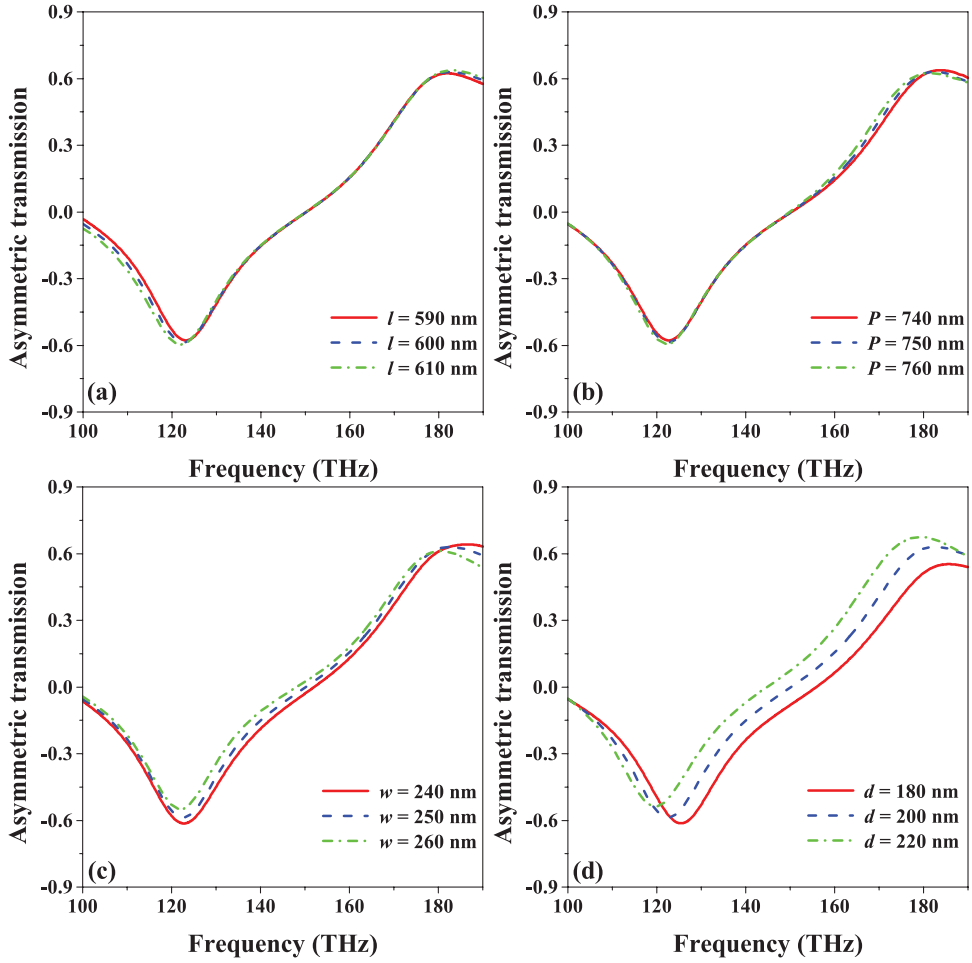

Figure 7. Asymmetric transmission with different a) length *l* of nanorod, b) period *P* of metasurface, c) width *w* of nanorod, and d) separation distance *d* of nanorod.

concise explanation for asymmetric transmission in few-layer metasurfaces. It releases the alignment requirement of adjacent nanorod layers and is useful in practical applications. The designed metasurface provides an intriguing design method for future polarization conversion devices based on asymmetric transmission. In addition, its diode-like asymmetric transmission in adjacent wavebands can lead to possible applications in information coding and decoding in the optical communication field.

Acknowledgements

This work was supported by the National Key Research and Development Program of China (2016YFA0301102), the National Basic Research Program (973 Program) of China (2012CB921900), the Natural Science Foundation of China (11574163, 61378006, and 11304163), and the Program for New Century Excellent Talents in University (NCET-13-0294).

Received: July 25, 2016
Revised: August 21, 2016
Published online:

[1] H. Cheng, Z. Liu, S. Chen, J. Tian, *Adv. Mater.* **2015**, *27*, 5410.
[2] N. Yu, F. Capasso, *J. Lightwave Technol.* **2015**, *33*, 2344.
[3] N. Yu, F. Capasso, *Nat. Mater.* **2014**, *13*, 139.
[4] N. I. Zheludev, Y. S. Kivshar, *Nat. Mater.* **2012**, *11*, 917.
[5] X. Chen, L. Huang, H. Mühlenbernd, G. Li, B. Bai, Q. Tan, G. Jin, C. W. Qiu, S. Zhang, T. Zentgraf, *Nat. Commun.* **2012**, *3*, 1198.
[6] M. Kang, T. Feng, H. T. Wang, J. Li, *Opt. Express* **2012**, *20*, 15882.
[7] L. Huang, X. Chen, H. Mühlenbernd, H. Zhang, S. Chen, B. Bai, Q. Tan, G. Jin, K. W. Cheah, C.-W. Qiu, *Nat. Commun.* **2013**, *4*, 2808.
[8] P. Genevet, N. Yu, F. Aieta, J. Lin, M. A. Kats, R. Blanchard, M. O. Scully, Z. Gaburro, F. Capasso, *Appl. Phys. Lett.* **2012**, *100*, 013101.
[9] P. Yu, S. Chen, J. Li, H. Cheng, Z. Li, W. Liu, B. Xie, Z. Liu, J. Tian, *Opt. Lett.* **2015**, *40*, 3229.
[10] N. Yu, F. Aieta, P. Genevet, M. A. Kats, Z. Gaburro, F. Capasso, *Nano Lett.* **2012**, *12*, 6328.
[11] H. Cheng, S. Chen, P. Yu, W. Liu, Z. Li, J. Li, B. Xie, J. Tian, *Adv. Opt. Mater.* **2015**, *3*, 1744.
[12] V. Fedotov, P. Mladyonov, S. Prosvirnin, A. Rogacheva, Y. Chen, N. Zheludev, *Phys. Rev. Lett.* **2006**, *97*, 167401.
[13] J. Shi, X. Liu, S. Yu, T. Lv, Z. Zhu, H. F. Ma, T. J. Cui, *Appl. Phys. Lett.* **2013**, *102*, 191905.
[14] Y. Xu, Q. Shi, Z. Zhu, J. Shi, *Opt. Express* **2014**, *22*, 25679.
[15] R. Singh, E. Plum, C. Menzel, C. Rockstuhl, A. Azad, R. Cheville, F. Lederer, W. Zhang, N. Zheludev, *Phys. Rev. B* **2009**, *80*, 153104.

[16] M. Mutlu, A. E. Akosman, A. E. Serebryannikov, E. Ozbay, *Phys. Rev. Lett.* **2012**, *108*, 213905.
[17] J. Shi, H. Ma, C. Guan, Z. Wang, T. Cui, *Phys. Rev. B* **2014**, *89*, 165128.
[18] Z. Li, S. Chen, C. Tang, W. Liu, H. Cheng, Z. Liu, J. Li, P. Yu, B. Xie, Z. Liu, *Appl. Phys. Lett.* **2014**, *105*, 201103.
[19] Z. Li, S. Chen, W. Liu, H. Cheng, Z. Liu, J. Li, P. Yu, B. Xie, J. Tian, *Plasmonics* **2015**, *10*, 1703.
[20] E. Plum, V. Fedotov, N. Zheludev, *Appl. Phys. Lett.* **2009**, *94*, 131901.
[21] J. Han, H. Li, Y. Fan, Z. Wei, C. Wu, Y. Cao, X. Yu, F. Li, Z. Wang, *Appl. Phys. Lett.* **2011**, *98*, 151908.
[22] Z. Wei, Y. Cao, Y. Fan, X. Yu, H. Li, *Appl. Phys. Lett.* **2011**, *99*, 221907.
[23] L. Wu, Z. Yang, Y. Cheng, M. Zhao, R. Gong, Y. Zheng, J. a. Duan, X. Yuan, *Appl. Phys. Lett.* **2013**, *103*, 021903.
[24] C. Pfeiffer, C. Zhang, V. Ray, L. J. Guo, A. Grbic, *Phys. Rev. Lett.* **2014**, *113*, 023902.
[25] CST Studio Suite, *Version 2015*, Computer Simulation Technology AG, Darmstadt, Germany **2015**.
[26] M. Ordal, L. Long, R. Bell, S. Bell, R. Bell, R. Alexander, C. Ward, *Appl. Opt.* **1983**, *22*, 1099.
[27] S. Zhang, W. Fan, K. J. Malloy, S. R. Brueck, N. C. Panoiu, R. M. Osgood, *J. Opt. Soc. Am. B* **2006**, *23*, 434.
[28] C. Menzel, C. Helgert, C. Rockstuhl, E.-B. Kley, A. Tünnermann, T. Pertsch, F. Lederer, *Phys. Rev. Lett.* **2010**, *104*, 253902.
[29] C. Menzel, C. Rockstuhl, F. Lederer, *Phys. Rev. A* **2010**, *82*, 053811.
[30] J. Vigoureux, R. Giust, *Opt. Commun.* **2000**, *186*, 21.
[31] N. K. Grady, J. E. Heyes, D. R. Chowdhury, Y. Zeng, M. T. Reiten, A. K. Azad, A. J. Taylor, D. A. Dalvit, H. T. Chen, *Science* **2013**, *340*, 1304.